water

MDPI

Article

Au/ZnO Hybrid Nanostructures on Electrospun Polymeric Mats for Improved Photocatalytic Degradation of Organic Pollutants

Laura Campagnolo [1,2], Simone Lauciello [3], Athanassia Athanassiou [1] and Despina Fragouli [1,*]

[1] Smart Materials, Istituto Italiano di Tecnologia, Via Morego 30, 16163 Genova, Italy
[2] Università degli Studi di Genova, Dipartimento di Chimica e Chimica Industriale, Via Balbi 5, 16126, Genova, Italy
[3] Electron Microscopy Facility, Istituto Italiano di Tecnologia, Via Morego 30, 16163 Genova, Italy

* Correspondence: despina.fragouli@iit.it; Tel.: +39-010-2896878 (D.F.)

Crystallite size approximation by Debye-Scherrer equation

The crystallite size was estimated by using the Debye-Scherrer equation (S1),

$$D_{hkl} = \frac{K\lambda}{\beta cos\theta_{hkl}} \quad \text{(S1)}$$

where D_{hkl} is the crystallite size (nm), K is a dimensionless factor referred to the crystallite shape, λ is the wavelength of the target (0.15406 nm for Cu), β is the Full-Width-Half-Maximum (FWHM) of the diffraction peak (rad) and θ_{hkl} is the diffraction peak angle. The presented crystallite sizes is the mean value obtained by the D_{hkl} values calculated from the three main diffraction peaks of the ZnO wurtzite phase at 31.8°, 34.3° and 36.1°.

Band gap energy extrapolation by Kubelka-Munk method

The band gap energy (E_g) was deduced from the diffuse reflectance spectra through the Kubelka-Munk (KM) function (S2),

$$F(R_\infty) = \frac{(1-R_\infty)^2}{2R_\infty} = \frac{K}{S} \quad \text{(S2)}$$

where $F(R_\infty)$ is the KM function, R_∞ is the absolute reflectance of the sample obtained by the ratio between the diffuse reflectance of the sample and the diffuse reflectance of the standard (MgO), K and S are the absorption and scattering coefficient respectively. Considering that E_g can be approximated from K as a function of the photon energy (hν) as shown in Equation S3,

$$K \propto \frac{(h\nu - E_g)^n}{h\nu} \quad \text{(S3)}$$

in which n is related to the type of optical transition, it is possible to determine E_g by plotting $(F(R_\infty)\cdot h\nu)^{1/n}$ as a function of hν and extrapolating the value from a linear regression of the straight part at $F(R_\infty) = 0$. In our case, the n value is defined to be ½, which is the value for a direct allowed transition, since it is well known that ZnO is a direct band gap semiconductor. The specific allowed or forbidden transition is experimentally determined from the best linear fit.

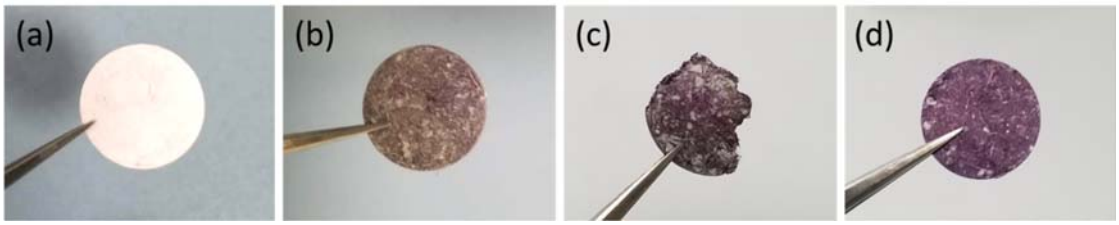

Figure S1. Photos of the (a) PMMA/ZnO, (b) PMMA/ZnO-Au1, (c) PMMA/ZnO-Au3 and (d) PMMA/ZnO-Au6.

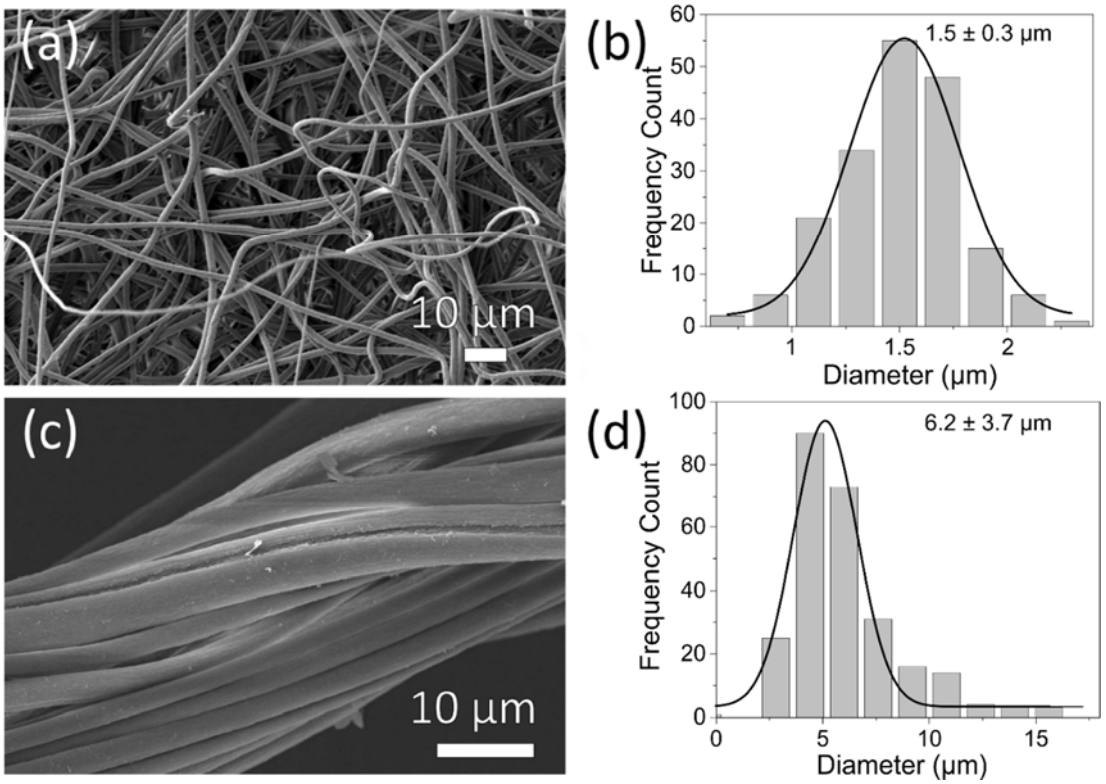

Figure S2. SEM images and size distribution analysis of the diameter of the fibers of the (a,b) PMMA and (c,d) PMMA/Zn(CH_3CO_2)$_2$ mats.

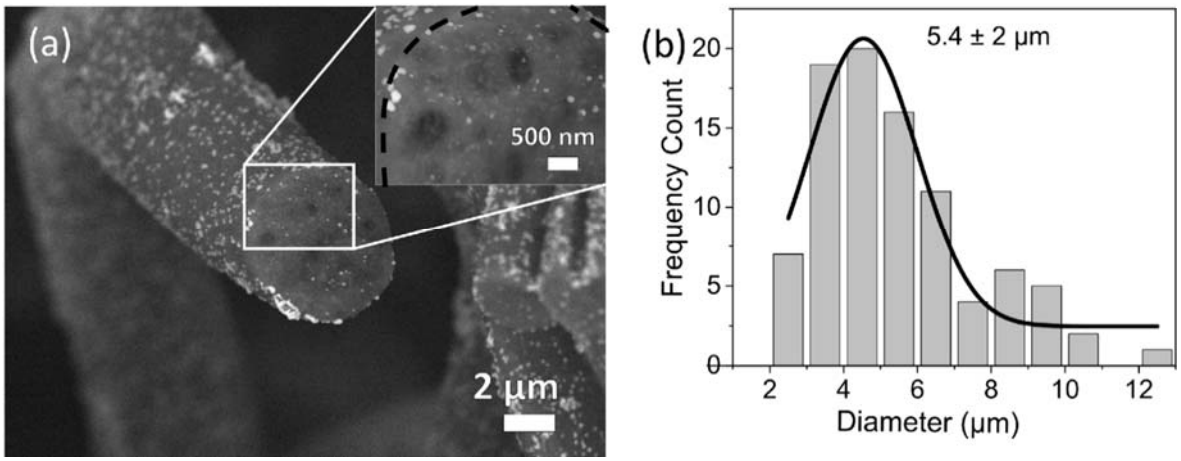

Figure S3**.** (a) HRSEM image of PMMA/ZnO with the cross-section detail. (b) Diameter size distribution of the PMMA/ZnO composite mat.

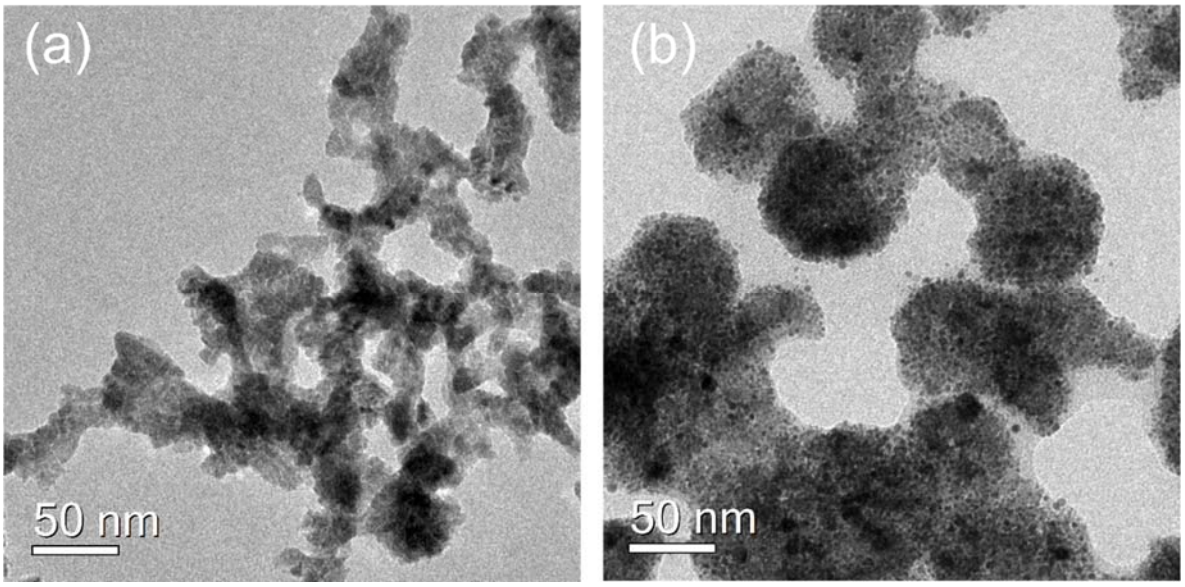

Figure S3. TEM images of the (a) smaller ZnO NPs formed in the bulk of the polymeric fibers and of the (b) ZnO/Au hybrid structure in the PMMA/ZnO-Au1 composite mat.

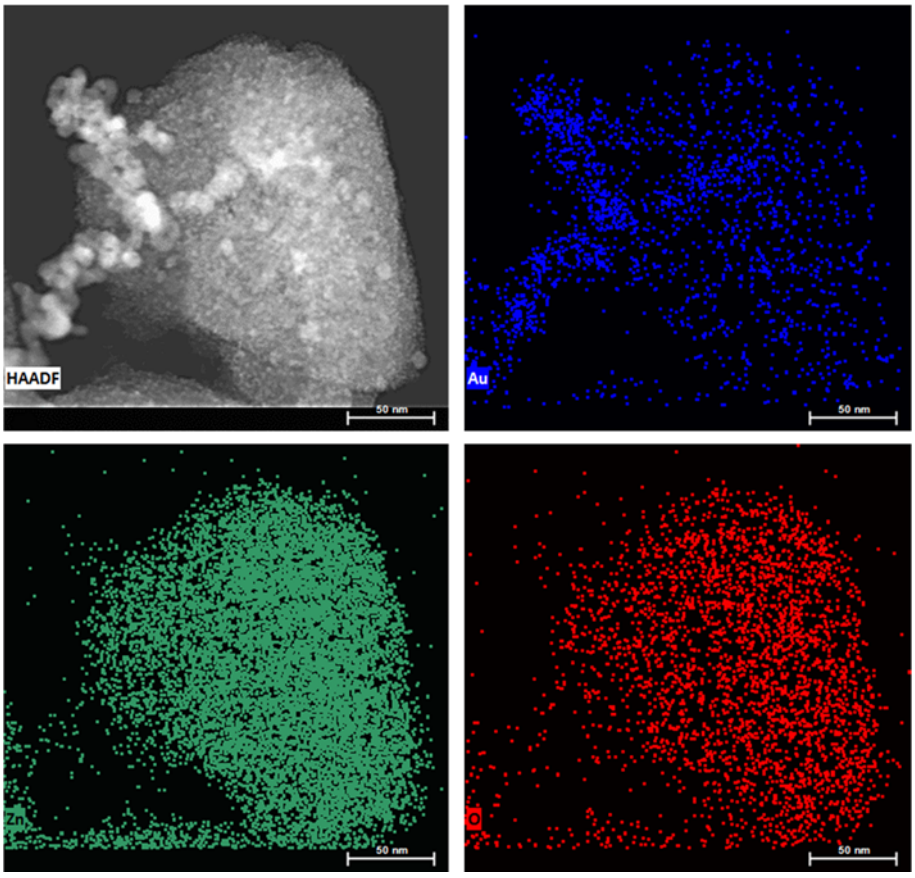

Figure S4. Dark field TEM image of the (a) ZnO-Au hybrid structure and EDS mapping of (b) Au, (c) Zn and (d) O.

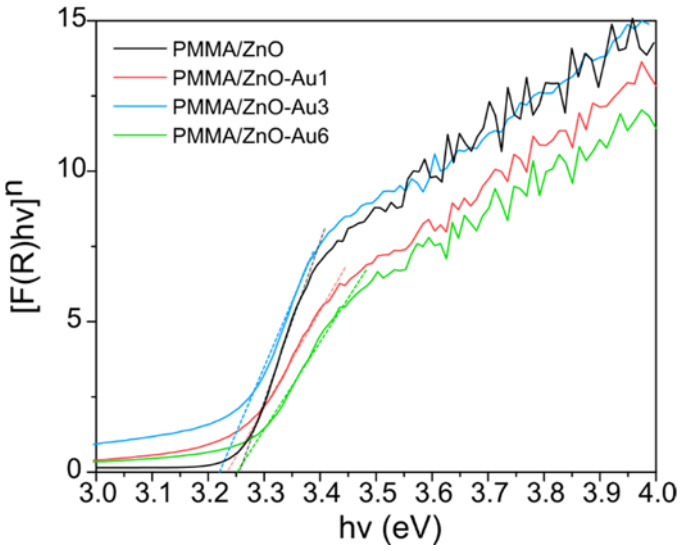

Figure S5. Kubelka-Munk plots of the composite mats. The energy band gap is extrapolate from a linear regression.

Table S1. Assignment of the Raman modes of the PMMA[1]

Raman shift (cm^{-1})	**Assignment**
482	C-C skeletal deformation of CC_4
559	O-C=O deformation
603	O-C=O deformation
735	O-C=O deformation coupled with CH_2 rocking
812	symmetric CC_4 stretching
838	C=O deformation coupled with CH_2 rocking
968	main chain C-C stretching
987	main chain C-C stretching
1059	CH_2 wagging
1122	C-O stretching coupled with CH_2 rocking
1158	C-O stretching coupled with CH_2 rocking
1185	C-C degenerate stretching of CC_4
1240	C-C degenerate stretching of CC_4
1391	CH_3 symmetric bending
1451	CH_2 deformation
1484	CH_3 asymmetric bending

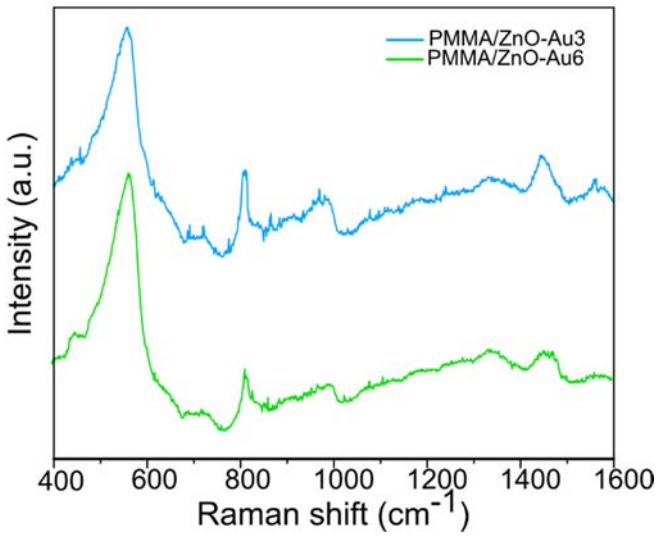

Figure S6. *Raman* spectra of PMMA/ZnO-Au3 and PMMA/ZnO-Au6

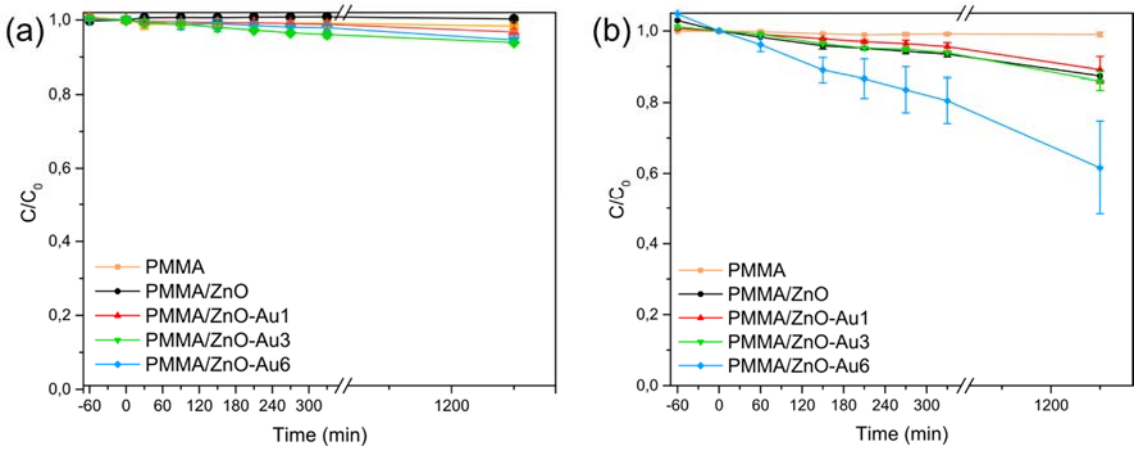

Figure S7. Evolution of the normalized concentration of (a) MB and (b) BPA solutions in presence of the developed mats in dark.

Table S 2. Degradation and mineralization values obtained from the photocatalytic degradation of the MB and BPA aqueous solution in presence of the mats after 20 h under UV light irradiation.

Samples	**MB**		**BPA**	
	%degradation	%mineralization	%degradation	%mineralization
PMMA/ZnO	77	45.5	34	-
PMMA/ZnO-Au1	88	60	63.5	15

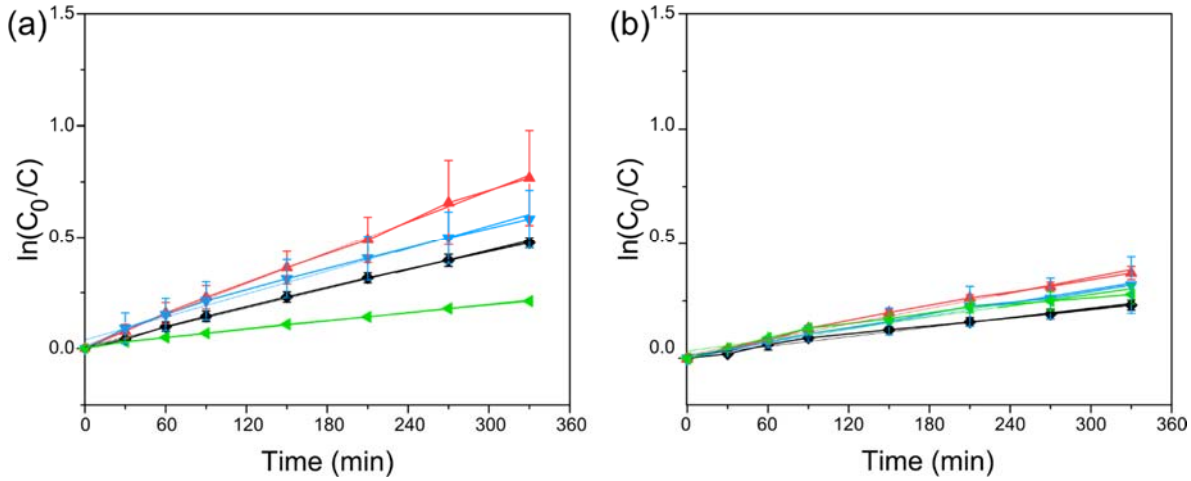

Figure S8. The pseudo-first-order reaction kinetics for (a) MB and (b) BPA, applied on the experimental data obtained in the first 5 hours of reaction.

Table S 3. Photo-degradation rate constants and linear regression coefficients obtained from the linear fitting of the experimental data by using the pseudo-first order model.

Samples	MB		BPA	
	10^{-3} k_1 (min^{-1})	R^2	10^{-3} k_1 (min^{-1})	R^2
PMMA/ZnO	1.44	0.9979	0.69	0.9820
PMMA/ZnO-Au1	2.33	0.9982	1.12	0.9895
PMMA/ZnO-Au3	1.71	0.9887	0.96	0.9923
PMMA/ZnO-Au6	0.63	0.9958	0.82	0.9478

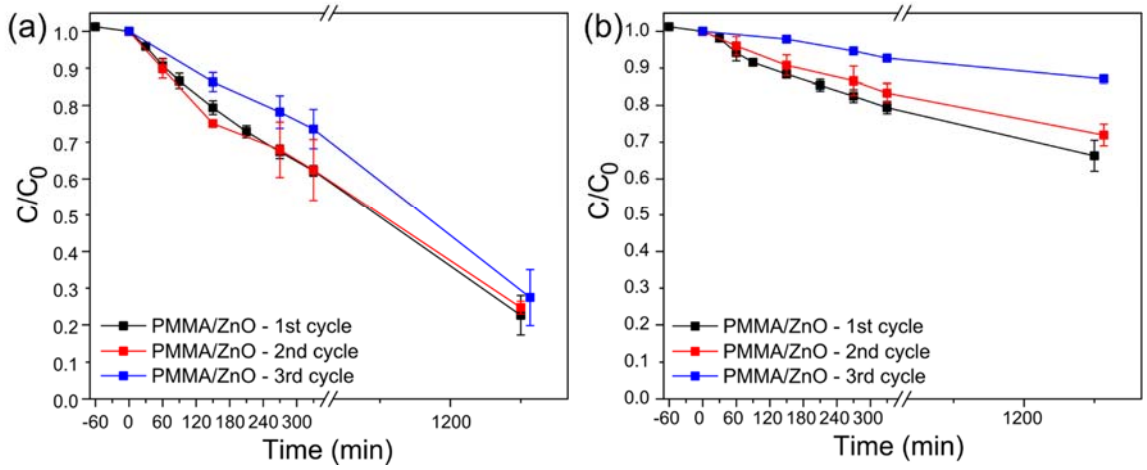

Figure S 9. Photocatalytic degradation activity of (a) MB and (b) BPA under UV light irradiation for three cycles using the PMMA/ZnO composite mat.

References

1 Akira, M.; Yanzhi, R.; Kimihiro, M.; Hiroshi, I.; Yukio, M.; Isao, N.; Yukihiro, O. Two-dimensional Fourier-transform Raman and near-infrared correlation spectroscopy studies of poly(methyl methacrylate) blends: 1. Immiscible blends of poly(methyl methacrylate) and atactic polystyrene. Vib. Spectrosc. 2000, 24, 171–180.